A&A 468, 1025–1031 (2007)
DOI: 10.1051/0004-6361:20065971

Astronomy & Astrophysics

Self-consistent theory of turbulent transport in the solar tachocline⋆

III. Gravity waves

Eun-jin Kim and N. Leprovost

Department of Applied Mathematics, University of Sheffield, Sheffield, S3 7RH, UK
e-mail: e.kim@sheffield.ac.uk

Received 5 July 2006 / Accepted 28 February 2007

ABSTRACT

Aims. To understand the fundamental physical processes important for the evolution of solar rotation and distribution of chemical species, we provide theoretical predictions for particle mixing and momentum transport in the stably stratified tachocline.
Methods. By envisioning that turbulence is driven in the tachocline, we compute the amplitude of turbulent flow, turbulent particle diffusivities, and eddy viscosity, by incorporating the effect of a strong radial differential rotation and stable stratification. We identify the different roles that the shear flow and stable stratification play in turbulence regulation and transport.
Results. Particle transport is found to be severely quenched due to stable stratification, as well as radial differential rotation, especially in the radial direction with an effectively more efficient horizontal transport. The eddy viscosity is shown to become negative for parameter values typical of the tachocline, suggesting that turbulence in the stably stratified tachocline leads to a non-uniform radial differential rotation. Similar results also hold in the radiative interiors of stars, in general.

Key words. Sun: interior – Sun: rotation – waves – turbulence

1. Introduction

On its journey on the main sequence, the sun has slowed down significantly due to the loss of angular momentum from its surface (e.g. see Stix 1989; Schatzman 1993). The angular momentum transport must have been very efficient during its spin-down in order for the sun to have the rotational profile observed today (see, e.g. Charbonneau et al. 1998). Vigorous turbulence in the convection zone and possibly thermal wind (Miesch et al. 2006) can readily provide a mechanism for efficient radial momentum transport, thereby eradicating radial differential rotation in it. Such turbulent transport is however considered to be absent in the stably stratified radiative interior, which has also spun-down during the solar evolution, presently rotating uniformly at a rate roughly the same as the mean average rotation rate on the solar surface. Whichever mechanism is responsible for momentum transport in the interior (which itself is an important problem), it should be closely related to the transport in the tachocline through which the surface spin-down is communicated to the interior. Transport in the tachocline also plays a crucial role in the overall mixing of light elements (lithium, beryllium, etc.) (see e.g. Schatzman 1993; Brun et al. 1999), thereby determining the level of their surface abundances on the sun. Therefore, it is essential to understand physical mechanisms for transport in the tachocline and then to formulate a consistent theory starting from first principles based on those processes. This is particularly true since virtually all the previous theoretical modelling heavily relies on a simple parameterisation of transport process, which is then adjusted to agree with observations.

We initiated the development of a consistent theory of turbulent transport in the tachocline in the previous papers, by taking into account the crucial effect of the large-scale shear flows provided by a strong radial differential rotation (Kim 2005), as well as latitudinal differential rotation (Leprovost & Kim 2006). By envisioning that the tachocline is perturbed externally – e.g. by plumes penetrating from the convection zone above (e.g. see Gilman 2000; Brummell et al. 2002; Rogers & Glazmaier 2005), or by instabilities (e.g. see Watson 1981; Charbonneau et al. 1999) –, we demonstrated how turbulence level and transport are reduced via shearing in a non-trivial manner (see also Burrell 1997; Kim 2004, 2006) in a simplified three-dimensional (3D) hydrodynamic turbulence. In particular, turbulent transport of chemical species and angular momentum are shown to become strongly anisotropic with much more efficient transport in the horizontal (latitudinal) direction than in the vertical (radial) direction due to shear stabilisation by a strong radial shear. The resulting anisotropic momentum transport was shown to reinforce a strong radial shear (Leprovost & Kim 2006), with positive feedback on the confinement of the tachocline (Spiegel & Zahn 1992), while chemical species are predicted to have latitudinal dependent mixing due to the variation in radial shear (Kim 2005). Furthermore, the results indicate that the turbulence regulation by a shear flow (i.e. differential rotation) leads to weak turbulence and mixing in turbulent tachocline.

The purpose of this paper is to investigate how a stable stratification in the tachocline modifies the predictions obtained in these studies. We again envision that the tachocline is turbulent, driven by a forcing as in Kim (2005). In the presence of a stable stratification, the turbulence in the tachocline is no longer completely random, as the stable stratification provides a restoring force against radial displacement of fluid elements, supporting the propagation of internal gravity waves (Lighthill 1978). These waves tend to increase the memory of otherwise random

⋆ Appendix A is only available in electronic form at http://www.aanda.org

turbulent fluid motion and can reduce the overall transport due to turbulence. We show that the turbulence quenching due to shear stabilisation found in previous studies is further enhanced in the presence of stable stratification (gravity waves). Thus, gravity waves acting together with shear stabilisation can lead to a weak mixing in the tachocline, as required for the surface depletion of lithiums (e.g. Pinsonneault et al. 1989).

It is important to contrast our approach to those adopted in most previous works, which focus on the momentum transport by gravity waves themselves through dissipative processes (e.g. Plumb 1978; Kim & MacGregor 2001, 2003; Talon et al. 2002). For instance, gravity waves are considered to be generated in the convection zone (Press 1981) and to deposit their momentum into background shear flow via radiative damping as they propagate through the tachocline and the interior (Kim & MacGregor 2001, 2003). Relying crucially on radiative damping, the momentum transport by gravity waves would occur on a long time scale (recall that the transport by waves requires molecular dissipation, and is thus a slow process). Similarly, weak mixing due to damped gravity waves was also suggested as a mechanism for a modestly enhanced mixing of light elements (lithium) (Press & Rybicki 1981; García López & Spruit 1991). In these works, a certain level of background turbulence could not be ruled out and was invoked to provide an enhanced viscosity for the evolution of a mean flow (Kim & MacGregor 2001, 2003) and the gravity waves (Charbonnel & Talon 2005; Talon et al. 2002). The value of the effective viscosity is often arbitrarily taken to be a positive constant, much larger than molecular viscosity and affected neither by shear flow nor by gravity waves, or it is simply parameterised.

In this paper, we treat turbulence and gravity waves on an equal footing and consistently compute the values of turbulent eddy viscosity and particle diffusivity by incorporating the effect of a shear flow (provided by a radial differential rotation) and identify different roles that gravity waves and shear flow play in turbulent transport. Specifically, we show that unlike shear flows, which reduce both turbulence level and transport, a stable stratification can suppress turbulent transport without much effect on turbulence level. We then demonstrate that the stratification favours a negative eddy viscosity and thus tends to sharpen the radial gradient of large-scale shear flows rather than smoothing it out. This tendency is also found in Kim & MacGregor (2001, 2003). We note that the elucidation of the effects of gravity waves is essential for understanding the momentum transport in the radiative interior, as they have often been advocated as a mechanism to explain a uniform rotation in that region. Stratified turbulence with a shear flow is also important for the transport in radiative interiors and/or envelops of stars, in general, as well as in geophysical systems. In particular, it has been studied actively in geophysical systems (e.g. see Jacobitz et al. 1997; Stacey et al. 1999), where stable stratification was shown to inhibit turbulent transport in the direction of a background density gradient, leading to 2D turbulence.

The remainder of the paper is structured as follows. We first investigate the effect of gravity waves on turbulence in Sect. 2. In Sect. 3, we incorporate the effect of strong radial differential rotation and study how the gravity waves modify the overall turbulent transport. Section 4 contains the conclusion and discussions.

2. Internal gravity waves

To simplify the problem, we consider incompressible fluid with local Cartesian coordinates x, y, and z for radial, azimuthal, and latitudinal directions, respectively (see Fig. 1), and use the Boussinesq approximation to capture the effect of stratification. We assume that the fluid is stirred by a forcing on small scales, giving rise to fluctuations. In the absence of stratification, this fluid forcing will drive turbulence on small scales and maintain it at the level at which the injected energy is balanced by dissipation in the system. As the stratification increases, the forcing will generate not only random turbulent motion but also coherent (gravity) waves. Alternatively, some of turbulent motion will be turned into packets of gravity waves. Therefore, we consider both turbulence and gravity waves as fluctuations on much smaller scales than those associated with mean density or mean background shear flows. Specifically, we express the total mass density $\rho = \rho_0(x) + \rho'$ where $\rho_0(x)$ and ρ' are the background and fluctuating mass densities, respectively; the total velocity $\boldsymbol{u} = \boldsymbol{U}_0 + \boldsymbol{v}$, where $\boldsymbol{U}_0$ and $\boldsymbol{v}$ are a large-scale shear flow due to differential rotation and small-scale fluctuations, and the total particle density of chemical elements $n = n_0(\boldsymbol{x}) + n'$ where $n_0(\boldsymbol{x})$ and n' are mean and fluctuating components. Then, the main governing equations for fluctuations $\boldsymbol{v}$, ρ', and n', involving both turbulence and gravity waves, are as follows (see, e.g., Kim & MacGregor 2003):

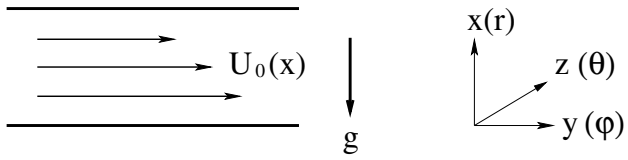

Fig. 1. The configuration of our model.

$$(\partial_t + \boldsymbol{U}_0 \cdot \nabla)\boldsymbol{v} = -\nabla p - g\rho'\hat{x} + \nu\nabla^2\boldsymbol{v} + \boldsymbol{f}, \quad (1)$$

$$\nabla \cdot \boldsymbol{v} = 0, \quad (2)$$

$$(\partial_t + \boldsymbol{U}_0 \cdot \nabla)\rho' = \frac{\overline{\rho}N^2}{g} v_x + \mu\nabla^2\rho', \quad (3)$$

$$(\partial_t + \boldsymbol{U}_0 \cdot \nabla)n' = -\partial_x n_0 v_x + D\nabla^2 n'. \quad (4)$$

Here, ν, μ, and D are molecular viscosity, thermal diffusivity, and particle diffusivity, respectively; $\boldsymbol{f}$ in Eq. (1) is the small-scale forcing driving turbulence; $\overline{\rho} = \rho_0(x = 0)$ is the constant background density [measured at the bottom of the convection zone (e.g. see Kim & MacGregor 2003)], and $N = \sqrt{-g(\partial_x\rho_0 + \overline{\rho}g/c_s^2)/\overline{\rho}}$ is the Brunt-Väisälä frequency, where c_s is the sound speed. Note that the typical values of ν, D, μ, and N in the tachocline are 10^2 cm^2 s^{-1}, 10^2 cm^2 s^{-1}, 10^7 cm^2 s^{-1}, and 3×10^{-3} s^{-1}, respectively.

In this section, we first ignore a background shear flow and study how the turbulence and transport are modified due to stable stratification in the tachocline. To obtain the overall turbulent transport, we solve coupled Eqs. (1)–(4) in terms of Fourier transform for fluctuating quantities ϕ':

$$\phi'(\boldsymbol{x}, t) = \frac{1}{(2\pi)^3}\int \mathrm{d}^3k\, \tilde{\phi}(\boldsymbol{k}, t) \exp\{i(k_x x + k_y y + k_z z)\}. \quad (5)$$

Equations (1)–(3) then give us an equation for $\tilde{\rho} = \mathrm{e}^{\nu k^2 t}\tilde{\rho}$ in the form

$$\partial_{tt}\tilde{\rho} + (\mu - \nu)k^2\tilde{\rho} + \overline{N}^2\tilde{\rho} = \frac{N^2}{g}\mathrm{e}^{\nu k^2 t}\tilde{h}_1. \quad (6)$$

Here, $\overline{N}^2 = \gamma N^2/(\gamma + a^2)$. Since $N \gg \mu k^2$ is valid on a broad range of reasonable scales $l \gg 10^4 \sim 10^5$ cm in

the tachocline, we can find the solutions to leading order in ($\nu k^2/N \ll$) $\mu k^2/N \ll 1$ as:

$$\tilde{v}_x \sim \frac{1}{\gamma + a^2} \int \mathrm{d}t' G_\mu(t,t') \cos \overline{N}(t-t') \tilde{h}_1(t'), \quad (7)$$

$$\tilde{v}_y \sim -\frac{a}{\gamma}\tilde{v}_x - \frac{\beta}{\gamma} \int \mathrm{d}t' G(t,t') \tilde{h}_2(t'), \quad (8)$$

$$\tilde{v}_z \sim -\frac{a\beta}{\gamma}\tilde{v}_x + \frac{1}{\gamma} \int \mathrm{d}t' G(t,t') \tilde{h}_2(t'), \quad (9)$$

$$\tilde{\rho} \sim \frac{N}{g\sqrt{\gamma(\gamma+a^2)}} \int \mathrm{d}t' G_\mu(t,t') \sin \overline{N}(t-t') \tilde{h}_1(t'). \quad (10)$$

Here, $G(t,t') = \mathrm{e}^{-\nu k^2 (t-t')}$ and $G_\mu(t,t') = \mathrm{e}^{-(\mu+\nu)k^2(t-t')/2}$ are the Green's functions; $a = k_x/k_y$, $\beta = k_z/k_y$, and $\gamma = 1+\beta^2$; $\tilde{h}_1$ and $\tilde{h}_2$ in Eqs. (6) and (7)–(10) are the forcing terms that are related to $\tilde{f}_i$ as

$$\tilde{h}_1 = (1+\beta^2)\tilde{f}_x - a\tilde{f}_y - a\beta\tilde{f}_z, \quad (11)$$

$$\tilde{h}_2 = -\beta\tilde{f}_y + \tilde{f}_z. \quad (12)$$

Equations (7)–(9) show that the vertical motion $\tilde{v}_x$, involving only G_μ, is always subject to radiative damping μ, while the horizontal motions $\tilde{v}_y$ and $\tilde{v}_x$, containing both G_μ and G, are much less affected by μ.

For simplicity, we assume the forcing to be homogeneous in space with a short correlation time τ_f:

$$\langle \tilde{f}_i(\boldsymbol{k}_1,t_1)\tilde{f}_j(\boldsymbol{k}_2,t_2)\rangle = \tau_f(2\pi)^3\delta(t_1-t_2)\delta(\boldsymbol{k}_1+\boldsymbol{k}_2)\,\psi_{ij}(\boldsymbol{k}_2). \quad (13)$$

Note that in the case where the forcing $\boldsymbol{f}$ due to plumes induces a stronger turbulence towards the bottom of the convection zone, $\boldsymbol{f}$ becomes inhomogeneous with the power spectrum $\psi_{ij} = \psi_{ij}(x,\boldsymbol{k})$ depending on the radial coordinate x.

A long but straightforward algebra by using Eqs. (7)–(13) then gives us the following results on turbulence level and particle diffusivity defined by $\langle n' v_i\rangle = -D_{\mathrm{T}}^{ij}\partial_j n_0$:

$$\langle v_x^2\rangle \sim \tau_f \int \frac{\mathrm{d}^3k}{(2\pi)^3} \frac{\phi_{11}(\boldsymbol{k})}{2(\gamma+a^2)^2} \frac{1}{(\mu+\nu)k^2}, \quad (14)$$

$$\langle v_y^2\rangle \sim \tau_f \int \frac{\mathrm{d}^3k}{(2\pi)^3} \Big[\frac{a^2\phi_{11}(\boldsymbol{k})}{2\gamma^2(\gamma+a^2)^2} \frac{1}{(\mu+\nu)k^2} + \frac{\beta^2\phi_{22}(\boldsymbol{k})}{\gamma^2}\frac{1}{2\nu k^2}\Big], \quad (15)$$

$$\langle v_z^2\rangle \sim \tau_f \int \frac{\mathrm{d}^3k}{(2\pi)^3} \Big[\frac{a^2\beta^2\phi_{11}(\boldsymbol{k})}{2\gamma^2(\gamma+a^2)^2} \frac{1}{(\mu+\nu)k^2} + \frac{\phi_{22}(\boldsymbol{k})}{\gamma^2}\frac{1}{2\nu k^2}\Big], \quad (16)$$

$$D_{\mathrm{T}}^{xx} \sim \frac{\tau_f}{N^2} \int \frac{\mathrm{d}^3k}{(2\pi)^3} \frac{\phi_{11}(\boldsymbol{k})}{4\gamma(\gamma+a^2)}, \quad (17)$$

$$D_{\mathrm{T}}^{yy} \sim \tau_f \int \frac{\mathrm{d}^3k}{(2\pi)^3\gamma^2} \left[\frac{a^2\phi_{11}(\boldsymbol{k})}{4\overline{N}^2(\gamma+a^2)^2} + \frac{\beta^2\phi_{22}(\boldsymbol{k})}{2\nu(\nu+D)^2k^4}\right], \quad (18)$$

$$D_{\mathrm{T}}^{zz} \sim \tau_f \int \frac{\mathrm{d}^3k}{(2\pi)^3\gamma^2} \left[\frac{a^2\beta^2\phi_{11}(\boldsymbol{k})}{4\overline{N}^2(\gamma+a^2)^2} + \frac{\phi_{22}(\boldsymbol{k})}{2\nu(\nu+D)^2k^4}\right]. \quad (19)$$

Here, we assume spatial symmetries $\phi_{ij}(k_y) = \phi_{ij}(-k_y)$ and $\phi_{ij}(k_y) = \phi_{ij}(-k_y)$; $\boldsymbol{k}$ inside the integrals in Eqs. (14)–(19) is the wavenumber of the forcing; $\phi_{ij}(\boldsymbol{k})$ ($i = 1,2$) is the power spectrum of the forcing defined by:

$$\langle \tilde{h}_i(\boldsymbol{k}_1,t_1)\tilde{h}_j(\boldsymbol{k}_2,t_2)\rangle = \tau_f(2\pi)^3\delta(t_1-t_2)\delta(\boldsymbol{k}_1+\boldsymbol{k}_2)\phi_{ij}(\boldsymbol{k}_2). \quad (20)$$

In this paper, we consider an incompressible forcing ($\nabla\cdot\boldsymbol{f} = 0$) for simplicity, in which case ϕ_{ij} in Eq. (20) is related to ψ_{ij} in Eq. (13) as:

$$\phi_{11} = \frac{k^4}{k_y^4}\psi_{11}, \phi_{12} = \frac{1}{k_y^4}\left(k^2k_xk_z\psi_{11} + k^2k_{\mathrm{H}}^2\psi_{13}\right),$$

$$\phi_{22} = \frac{1}{k_y^4}\left(k_x^2k_z^2\psi_{11} + k_{\mathrm{H}}^4\psi_{33} + 2k_xk_zk_{\mathrm{H}}^2\psi_{13}\right). \quad (21)$$

Note that ϕ_{11} and ϕ_{22} can signify strong radial forcing and horizontal forcing, respectively. For instance, in the case of strong radial forcing by plumes ($\psi_{11} \gg \psi_{33}$) with $k_{\mathrm{H}} \gg k_x$ (see Fig. 2 in Leprovost & Kim 2006), ϕ_{11} will dominate ϕ_{22}. Note further that in the 2D limit with $k_z = 0$ and $\psi_{33} = 0$, ϕ_{22} vanishes.

We discuss some of the important implications of Eqs. (14)–(19). First, all three components of fluctuating velocity amplitude in Eqs. (14)–(17) are independent of N, clearly showing that the amplitude of the turbulent flow is not influenced by stable stratification in the case of the forcing with a short correlation time. The exact level of fluctuations is determined by the characteristics of the external forcing (ϕ_{ij}). We examine this in the simple 2D limit where $k_z = 0$ ($\gamma = 1$) and $\psi_{33} = 0$. In this limit, the substitution of $\phi_{22} = 0$ in Eqs. (14)–(17) gives $\langle v_x^2\rangle/\langle v_y^2\rangle \sim 1/a^2 = k_y^2/k_x^2$ and $\langle v_z^2\rangle = 0$. This is an expected result for the 2D incompressible fluid in the $x-y$ domain.

If the forcing $\boldsymbol{f}$ contains only gravity modes, the wave number of the forcing would satisfy the local dispersion relation $k_x = \pm k_y\sqrt{N^2/(\omega - U_0k_y)^2 - 1}$ (here, ω is the frequency of the gravity waves). Furthermore, if these gravity modes are generated by the overturning of fluids in the convection zone (e.g. Press 1981) with $U_0 \sim 0$, they would have strong power at low frequencies $\omega \ll N$, thereby giving $k_x/k_y \sim N/\omega \gg 1$, and thus $\langle v_x^2\rangle/\langle v_y^2\rangle \ll 1$. Note that this is the situation normally considered in the previous works (e.g. Kim & MacGregor 2001, 2003; Talon et al. 2002), where the main focus is on the momentum deposition by such gravity waves due to radiative damping after entering the tachocline from the bottom of the convection zone.

In contrast, in this paper, the forcing $\boldsymbol{f}$ is not restricted to gravity modes, but is taken to be general, including any form of perturbation with arbitrary values of k_x/k_y. For instance, in the case of a strong radial forcing due to plumes with $\phi_{11} \gg \phi_{22}$ and $a = k_x/k_y \ll 1$ (see Fig. 2 in Leprovost & Kim 2006), $\langle v_x^2\rangle/\langle v_y^2\rangle \gg 1$ with a stronger radial fluctuation than horizontal one. Furthermore, Eqs. (14)–(17) show that the level of anisotropy measured by the ratio of the turbulence amplitude depends on ν and μ. For instance, for an isotropic forcing with $\phi_{11} \sim \phi_{22}$, $\langle v_x^2\rangle/\langle v_y^2\rangle \propto \nu/\mu \ll 1$ becomes small as the radiative damping μ increases. This is because a high μ tends to decrease (vertical) turbulence level by introducing large (thermal) dissipation. Thus, without a shear flow, a stronger horizontal turbulence (level) than vertical one can be caused by high thermal diffusivity μ (but not by stratification) in the case of a temporally short correlation forcing. Note that the anisotropy in turbulence level could be related to the Peclet number $\mathrm{Pe} = vl/\mu$ as $\langle v_x^2\rangle/\langle v_y^2\rangle \propto \mathrm{Pe}$. Here, v and l are the characteristic velocity and the length scale of the forcing (which is fixed).

Second, turbulent transport in Eqs. (17)–(19) are strongly affected by stratification as N^2 increases, in contrast to fluctuation levels in Eqs. (14)–(17). Since $N \gg \mu k^2$ on reasonable scales $l \gg 10^4 \sim 10^5$ cm, the vertical (radial) mixing is severely quenched as the stratification increases (i.e. as N^{-2}), in qualitative agreement with Brun et al. (1999). In comparison, the part of the horizontal (latitudinal) mixing due to the radial forcing ϕ_{11}

is reduced proportional to N^{-2}, while the one due to the horizontal forcing ϕ_{22} is independent of N. The comparison of these two contributions (or alternatively D_{xx} and D_{yy}) in the case of $\phi_{11} \sim \phi_{22}$ gives us a cut-off scale $l_c \sim \sqrt{\nu/N}$ above which vertical (radial) mixing is strongly reduced compared to the horizontal (latitudinal) mixing. That is, in the presence of both radial and horizontal forcings of comparable strength, stable stratification mainly reduces the vertical transport without much effect on horizontal transport on scales $l > l_c$. For parameter values typical of the tachocline $\nu \sim 10^2$ cm^2 s^{-1} and $N \sim 3 \times 10^{-3}$ s^{-1}, $l_c \sim 10^2$ cm. Thus, the stratification is very likely to play an important role over a broad range of physically reasonable scales. Within the limit of strong radial forcing with $\phi_{11} \gg \phi_{22}$ and $a \sim 0$, the stratification influences both the radial and horizontal transports to the same degree, while the incompressibility renders $D_T^{xx}/D_T^{yy} \sim D_T^{xx}/D_T^{zz} \sim 1/a^2 \sim \langle v_x^2\rangle/\langle v_y^2\rangle \gg 1$, with an effectively more efficient radial transport. It is interesting to compare our result $D_{xx} \propto N^{-2}$ with the mixing due to radiatively damped waves (e.g. García López & Spruit 1991; Talon et al. 2002). For instance, García López & Spruit (1991) estimated the vertical mixing due to gravity waves to be proportional to μ/N^2. While the reduction in vertical mixing for large N qualitatively agrees with our results ($\propto N^{-2}$), the increase in vertical mixing in García López & Spruit (1991) is due to the fact that damped waves are necessary for wave transport.

Finally, we note that without a shear flow, momentum transport vanishes (i.e. $\langle v_x v_y\rangle = \langle v_x v_z\rangle = 0$) for an isotropic forcing. Scaling of turbulence amplitude, turbulent viscosity (ν_T), and turbulent diffusivity D_T are summarised in Table 1 for an isotropic forcing.

A high thermal diffusivity ($\mu = 10^5\nu$) in the tachocline is often considered to reduce the stabilising effect of stable stratification via the weakening of the buoyancy restoring force. To highlight this effect, it is illuminating to consider the extreme limit of strong thermal diffusion where density fluctuation becomes stationary with $\partial_t\rho' = N^2 v_x/g - \mu k^2\rho' = 0$ in Eq. (3). In this limit, by following a similar analysis as previously (with $D = \nu$), we can easily obtain the vertical and horizontal particle diffusivities as follows:

$$D_{xx} \sim \frac{\tau_f}{2\alpha^2}\int \frac{d^3k}{(2\pi)^3}\frac{\phi_{11}(\boldsymbol{k})}{(\gamma + a^2)^2}, \tag{22}$$

$$D_{yy} \sim \tau_f \int \frac{d^3k}{(2\pi)^3\gamma^2}\left[\frac{a^2\phi_{11}(\boldsymbol{k})}{\gamma^2(\gamma+a^2)^2}\frac{1}{2\alpha^2} + \frac{\beta^2\phi_{22}(\boldsymbol{k})}{(2\nu k^2)^2}\right], \tag{23}$$

where $\alpha = \gamma N^2/\mu k^2(\gamma + a^2)$. Equation (22) shows that the vertical mixing $D_{xx} \propto \mu^2/N^4 \propto \mathrm{Pe}^{-2}$ decreases for large N while increasing for large μ. This is because the reduction in the vertical mixing due to buoyancy force is weakened by a strong radiative damping μ. The comparison of Eqs. (22)–(23) further shows that the reduction in vertical mixing relative to horizontal mixing is given by a factor of $(\nu k^2)^2/\alpha^2$ for an isotropic forcing and is thus weaker than in the case of weak radiative damping $\mu k^2 \ll N$ (see Eqs. (17)–(19)). Furthermore, this reduction appears on scales larger than the critical scale $l_{c\mu} = (\mu\nu)^{1/4}/N^{1/2} \sim 10 l_c$. Here, $l_c = \sqrt{\nu/N}$ is the critical scale in the case of $\mu k^2 \ll N$. These results thus show that a strong thermal diffusion weakens the buoyancy effect and makes the effect of stratification become important on larger scales, compared to the case of a weak thermal diffusion. This result thus confirms with the expectation employed in previous works.

To summarise, a stable stratification can dramatically quench turbulent transport with a more effective mixing in the horizontal directions orthogonal to the background density gradient. It does not, however, affect the amplitude of the turbulent flow, the ratio of which is found to depend only on ν/μ (for a temporally short-correlated forcing).

Table 1. Scaling of turbulence amplitude, turbulent viscosity (ν_T), and turbulent diffusivity D_T for an isotropic forcing with $\phi_{11} \sim \phi_{22}$ in the case $N \gg \mu k^2$ and $D \sim \nu \ll \mu$. The quantities $\xi_\mu = \mu k_y^2/\mathcal{A} \ll 1$, $\xi_\nu = \nu k_y^2/\mathcal{A} \ll 1$, and $\xi_D = Dk_y^2/\mathcal{A} \ll 1$ are small parameters representing strong shear limit. The second ($\mathcal{A} = 0$ and $N \neq 0$), the third ($\mathcal{A} \neq 0$ and $N = 0$), and the fourth ($\mathcal{A} \neq 0$ and $N \neq 0$) columns contain the results for the stratified unsheared case in Sect. 2, for unstratified sheared case (Kim 2005), and for stratified sheared case in Sect. 3, respectively.

	$\mathcal{A} = 0, N \neq 0$	$\mathcal{A} \neq 0, N = 0$	$\mathcal{A} \neq 0, N \neq 0$
$\langle v_x^2\rangle$	μ^{-1}	$\mathcal{A}^{-1}$	$\mathcal{A}^{-1}$
$\langle v_y^2\rangle \sim \langle v_z^2\rangle$	ν^{-1}	$\mathcal{A}^{-1}\xi_\nu^{-1/3}$	$\mathcal{A}^{-1}\xi_\nu^{-1/3}$
ν_T	0	$\mathcal{A}^{-2}$	$-\mathcal{A}^{-2}$
D_T^{xx}	N^{-2}	$\mathcal{A}^{-2}$	$N^{-2}\xi_D\xi_\mu^{-2/3}$
$D_T^{yy} \sim D_T^{zz}$	$\nu^{-1}(\nu + D)^{-1}$	$\mathcal{A}^{-2}\xi_\nu^{-2/3}$	$\mathcal{A}^{-2}\xi_\nu^{-2/3}$
$\langle v_y^2\rangle/\langle v_x^2\rangle$	μ/ν	$\xi_\nu^{-1/3}$	$\xi_\nu^{-1/3}$
D_T^{yy}/D_T^{xx}	N^2	$\xi_\nu^{-2/3}$	$(N/\mathcal{A})^2(\mu/\nu)^{2/3}\xi_\nu^{-1}$

3. Consistent theory

The results in Sect. 2 show that for a temporally short correlated forcing, a stable stratification only reduces turbulent transport, leading to anisotropic turbulent transport, without much effect on turbulence level. In this section, we study how these results are modified by a stable background shear flow (differential rotation in the tachocline). In particular, we will show that a shear flow not only inhibits the vertical mixing further, enhancing the anisotropic transport, but also reduces turbulence levels anisotropically, thereby leading to stronger horizontal turbulence. For simplicity, we ignore the latitudinal differential rotation compared with the radial differential rotation since it is weaker in the tachocline due to a thin tachocline ($h < 0.03 \sim 0.05$ of the solar radius R). The inclusion of the latitudinal differential rotation would introduce a small correction term into our results. For instance, for turbulence amplitude, this correction term is roughly $(h/R)^2 \ll 1$, as shown in Leprovost & Kim (2006). Note that the latitudinal shear is crucial for non-vanishing horizontal momentum transport in Leprovost & Kim (2006). Again, we envision that turbulence is maintained in the tachocline by an external forcing, while gravity waves are excited due to this external forcing in the stably stratified tachocline. We then compute the overall turbulent transport consistently by taking the interaction among turbulence, shear flow, and gravity waves into account, instead of simply assuming a (high) constant value of turbulent viscosity for the mean shear flow (and gravity waves). Note that this treatment is essential when there is no clear scale separation between gravity waves and turbulence, in which case turbulence cannot be considered to give an enhanced value of viscosity for gravity waves (cf. Charbonnel & Talon 2005).

For the evolution of fluctuations, we approximate the radial differential rotation by a linear shear flow with $\boldsymbol{U}_0 = -x\mathcal{A}\hat{y}$ to keep the analysis tractable. Here, $\mathcal{A}$ is the shearing rate that we assume to be positive without loss of generality. As in previous papers (Kim 2005; Leprovost & Kim 2006), to capture the effect of shearing due to radial differential rotation ($\mathcal{A} \sim 3 \times 10^{-6}$ s^{-1}

for the tachocline) non-perturbatively, we use the special Fourier transform for fluctuating quantities ϕ':

$$\phi'(\boldsymbol{x},t) = \frac{1}{(2\pi)^3}\int \mathrm{d}^3k\tilde{\phi}(\boldsymbol{k},t)\exp\{\mathrm{i}(k_x(t)x + k_y y + k_z z)\}. \quad (24)$$

Here, $k_x = k_x(t)$ is the time dependent, unlike constant k_x in Eq. (5), satisfying an eikonal equation

$$\partial_t k_x(t) = k_y\mathcal{A}. \quad (25)$$

Equation (25) implies that k_x linearly increases in time as $k_x(t) = k_x(0) + k_y\mathcal{A}t$, manifesting the main effect of shearing by a shear flow $U_0(x)\hat{y}$, i.e., generation of fine scales in the x direction due to tilting and distortion of fluid eddies (e.g. see Burrell 1997; Kim 2004; Kim 2005). The efficient generation of fine scales by shearing leads to the breakup of eddies and enhancement of the overall dissipation, thereby reducing turbulence amplitude and transport (e.g. see Kim 2005). A similar effect by a shear flow is expected to persist for a more realistic radial shear (e.g. for an error function used in helioseismic inversions: Kosovichev 1996; Corbard et al. 1999) since the basic mechanism of shearing (e.g. see Fig. 2 in Kim 2005) is the same regardless of the details of the profile of radial shear provided that it is stable. The efficiency of the shearing could depend on the details of the profile, possibly leading to a slightly different scaling.

It is interesting to note that a gravity wave with an initially positive value of $k_x(0)$ can change its sign after the time interval $k_x(0)/k_y\mathcal{A}$ (for $k_y > 0$) due to shearing. Since the local (radial) group velocity of gravity waves is given by $v_{gx} = -k_y^2k_xN^2/k^4(\omega - U_0k_y)$ (e.g., see Kim & MacGregor 2003), the gravity wave alters its propagation direction as k_x flips its sign. Therefore, a gravity wave that initially propagates downward to the interior from the convection zone with a negative vertical group velocity (i.e. $v_{gx} < 0$) can propagate upwards when the vertical group velocity becomes positive ($v_{gx} > 0$) due to shearing.

For parameter values typical of the tachocline $N \sim 3\times10^{-3}$ s^{-1} and $\mathcal{A} \sim 3\times10^{-6}$ s^{-1}, $Ri = N^2/\mathcal{A}^2 \gg Ri_c \simeq 1/4$, satisfying the stability criterion (Lighthill 1978). We thus assume that the radial shear flow is stable with a high value of $Ri = N^2/\mathcal{A}^2 \gg 1$ in the rest of the paper (see also Schatzman et al. 2000). Note that the buildup of the chemical composition gradient [the so-called μ gradient in the solar interior (e.g. see Michaud & Zahn 1998, and references therein)] would further increase the values of N and Ri, making the radial shear flow stabler, although this effect could be counteracted by a radiative damping, as shown in Sect. 2. The shearing rate $\mathcal{A} \sim 3\times10^{-6}$ s^{-1} due to this radial differential rotation is higher than the dissipation rate due to radiative damping μk_y^2 on a broad range of scales $l(=1/k_y) > 10^6 \sim 10^7$ cm $\sim 10^{-3}H_0$, where H_0 is the pressure scale height $\sim 6\times10^9$ cm. Thus, we focus on the strong shear limit in the following by using $\xi_\mu = \mu k_y^2/\mathcal{A} \ll 1$ as a small parameter.

For $Ri \gg 1$ and $\nu \sim D \ll \mu$, a long but straightforward algebra can give us the solutions to Eqs. (1)–(4), as shown in Appendix A. By using these solutions and the correlation functions of forcing defined in Eq. (20), we obtain the following results for the turbulence level and transport coefficient defined by $\langle n'v_i\rangle = -D_{\mathrm{T}}^{ij}\partial_j n_0$ for $i = 1, 2$, and 3, and momentum flux $\langle v_xv_y\rangle = -\nu_{\mathrm{T}}\partial_x U_0$ in the strong shear limit $\xi_\mu = \mu k_y^2/\mathcal{A} \ll 1$ (see Appendix A for details):

$$\langle v_x^2\rangle \simeq \frac{\tau_f}{\mathcal{A}}\int\frac{\mathrm{d}^3k}{(2\pi)^3}\frac{\phi_{11}(\boldsymbol{k})}{2\gamma^{3/2}}, \quad (26)$$

$$\langle v_y^2\rangle \simeq \frac{\tau_f}{\mathcal{A}}\int\frac{\mathrm{d}^3k}{(2\pi)^3}\left[\frac{\phi_{11}(\boldsymbol{k})}{2\gamma^{5/2}}|\ln\xi_\mu| + \frac{\beta^2\phi_{22}(\boldsymbol{k})}{\gamma^2}G_0\right], \quad (27)$$

$$\langle v_z^2\rangle \simeq \frac{\tau_f}{\mathcal{A}}\int\frac{\mathrm{d}^3k}{(2\pi)^3}\left[\frac{\beta^2\phi_{11}(\boldsymbol{k})}{2\gamma^{5/2}}|\ln\xi_\mu| + \frac{\phi_{22}(\boldsymbol{k})}{\gamma^2}G_0\right], \quad (28)$$

$$D_{\mathrm{T}}^{xx} \simeq \frac{\tau_f}{2N^2}\int\frac{\mathrm{d}^3k}{(2\pi)^3}\frac{\phi_{11}(\boldsymbol{k})}{\gamma\sqrt{\gamma+a^2}}\xi_D G_1, \quad (29)$$

$$D_{\mathrm{T}}^{yy} \simeq \frac{\tau_f}{2}\int\frac{\mathrm{d}^3k}{(2\pi)^3\gamma^2}\left[\frac{\phi_{11}(\boldsymbol{k})\Gamma(\frac{4}{3})}{2N^2\gamma\sqrt{\gamma+a^2}}\frac{D}{\mu}\left(\frac{3}{\xi_\mu}\right)^{\frac{1}{3}} + \frac{\beta^2\phi_{22}(\boldsymbol{k})\Gamma(\frac{5}{3})}{\mathcal{A}^2}\left(\frac{3}{2\xi_\nu}\right)^{\frac{2}{3}}\right], \quad (30)$$

$$\nu_{\mathrm{T}} \simeq -\frac{\tau_f}{2}\int\frac{\mathrm{d}^3k}{(2\pi)^3}\frac{\phi_{11}(\boldsymbol{k})}{\gamma(\gamma+a^2)}\left[\frac{1}{\mathcal{A}^2} + \frac{1}{12N^2(\gamma+a^2)}\right]. \quad (31)$$

Here, $\xi_\nu = \nu k_y^2/\mathcal{A} \ll 1$, $\xi_D = Dk_y^2/\mathcal{A} \ll 1$, $\xi_\mu = \mu k_y^2/\mathcal{A} \ll 1$, $G_0 = \frac{1}{3}\Gamma(1/3)(3/2\xi_\nu)^{1/3}$, and $G_1 = \frac{1}{3}\Gamma(2/3)\left(3/\xi_\mu\right)^{2/3}$. Note again that $\xi_\mu \ll 1$ is valid on a broad range of scales $l(=1/k_y) > 10^6 \sim 10^7$ cm in the tachocline and also that $\xi_\mu \ll 1$ guarantees that $\xi_D \sim \xi_\nu \ll 1$ since $D \sim \nu \ll \mu$. The spectrum ϕ_{ij} in Eqs. (26)–(31) are given by Eqs. (20), which are related to the power spectrum of forcing ψ_{ij} in Eq. (13) in the incompressible case.

Equations (26)–(31) reveal the following interesting features. Turbulence levels given in Eqs. (26)–(28) are independent of stratification, similar to the case without a shear flow [Eqs. (14)–(17)], while they are reduced for strong shear $\mathcal{A}$. This indicates that waves and shear flows play different roles in turbulence regulation – waves do not necessarily quench fluctuation levels, while shear flows can reduce them through enhanced dissipation via shearing. The turbulence regulation by shearing gives us horizontal velocity fluctuations in Eqs. (27) and (28), which are effectively higher than the vertical one in Eq. (26). While a similar tendency was also found in the absence of gravity waves (Kim 2005), the exact value of the ratio of vertical to horizontal turbulence levels is not the same. For example, $\langle v_x^2\rangle/\langle v_y^2\rangle \propto (|\ln\xi_\mu|)^{-1}$ for a strong radial forcing ϕ_{11} with $\phi_{22} = 0$, while $\langle v_x^2\rangle/\langle v_y^2\rangle \propto \xi_\nu^{1/3}$ for an isotropic forcing with $\phi_{11} \sim \phi_{22}$. Note that $\xi_\nu \ll \xi_\mu \ll 1$ are small parameters in our problem, representing the strong shear limit. These results are to be compared with $\langle v_x^2\rangle/\langle v_y^2\rangle \propto \xi_\nu^{1/3}$ in the unstratified medium (Kim 2005). The results for the isotropic forcing in various cases are summarised and compared in Table 1.

Transport properties in Eqs. (29)–(31), however, exhibit a very different behaviour, with both vertical and horizontal mixing being inhibited in a non-trivial manner by strong stratification, as well as by shearing. First, the vertical transport is reduced as $D_{\mathrm{T}}^{xx} \propto \xi_D\xi_\mu^{-2/3}N^{-2} \propto D\mu^{-2/3}\mathcal{A}^{-1/3}N^{-2}$, becoming small as either stratification or shearing increases. Note that the decrease in D_{T}^{xx} for large N agrees with Miesch (2003). Interestingly, $D_{\mathrm{T}}^{xx} \propto \mu^{-2/3} \propto \mathrm{Pe}^{2/3}$ decreases as the radiative damping μ increases. This is because large radiative damping increases thermal dissipation, thereby mainly inhibiting the vertical mixing, as noted in Sect. 2. Thus, compared to the case with $N = 0$ where $D_T^{xx} \propto \mathcal{A}^{-2}$ (Kim 2005), the vertical mixing is much more quenched by a factor of $\xi_D\xi_\mu^{-2/3}(\mathcal{A}/N)^2 \ll \xi_D\xi_\mu^{-2/3} = (D/\mu)\xi_\mu^{1/3} \ll \xi_\mu \ll 1$ since $\mathcal{A}/N < 1$ and $D/\mu \sim 10^{-5}$ in the tachocline (see also Table 1). This clearly shows that shear flow (orthogonal to radial density gradient), stable stratification, and radiative damping can all inhibit the radial transport.

Second, $D_{\rm T}^{yy}$ is less affected by stratification since it involves the two parts; the one from ϕ_{11} is proportional to $\xi_D\xi_\mu^{-4/3}N^{-2}$, while the other from ϕ_{22} is proportional to $\mathcal{A}^{-2}\xi_\nu^{-2/3}$, independent of N. In the simplest case of a strong radial forcing with $\phi_{22} = 0$, $D_{\rm T}^{xx}/D_{\rm T}^{yy} \sim \xi_\mu^{2/3} \ll 1$, independent of N. This is similar to the case without stratification where $D_{\rm T}^{xx}/D_{\rm T}^{yy} \sim \xi_\nu^{2/3}$ (Kim 2005). In the general case where $\phi_{11} \neq 0$ and $\phi_{22} \neq 0$, $D_{\rm T}^{yy}$ exhibits a non-trivial, complex interplay among stratification and shear flow in determining the overall transport. To appreciate this, we compare Eq. (31) with the result obtained without shear flow (18) to find that shear flow enhances the contribution from ϕ_{11} by a factor $\xi_D\xi_\mu^{-4/3} = (D/\mu)\xi_\mu^{-1/3}$, while it reduces the part from ϕ_{22} by a factor of $(\nu/\mathcal{A})^2\xi_\nu^{-2/3} \propto \xi_\nu^{4/3} \ll 1$. Since $D/\mu \sim 10^{-5} \ll 1$ and $\xi_\mu \ll 1$, the horizontal transport driven by a strong radial forcing ϕ_{11} can be either inhibited or enhanced by a shear flow (due to ϕ_{11}) depending on the parameter values. On the other hand, the horizontal transport due to ϕ_{22} is reduced by the shear flow by a factor proportional to $\xi_\nu^{4/3} \ll 1$. The end result can easily be shown to be the enhancement of the effect of stratification. To see this, we compare the two contributions from ϕ_{11} and ϕ_{22} to $D_{\rm T}^{yy}$ and obtain a characteristic scale $l_* = (D/\mu)^2(\nu/N)^{1/2}(\mathcal{A}/N)^{5/2}$ above which the stratification is important, mainly responsible for quenching transport. Since l_* is smaller than $l_{\rm c} = (\nu/N)^{1/2}$ obtained without a shear flow, the effect of stratification becomes important compared to the case without shear flows. It is also worth comparing the contributions to $D_{\rm T}^{yy}$ from ϕ_{11} and ϕ_{22} separately to those in the case of $N = 0$ in Kim (2005), where $D_{\rm T}^{yy} \propto \mathcal{A}^{-2}\xi_\nu^{-2/3}$ from both ϕ_{11} and ϕ_{22}. That is, the contribution from ϕ_{11} is further reduced by a factor of $(\mathcal{A}/N)^2\xi_\nu^{1/3}(\nu/\mu)^{4/3}$ by stratification, while the one from ϕ_{22} is not affected.

We now examine how the stratification affects the anisotropy in transport. Equations (29) and (31) for a strong radial forcing with $\phi_{11} \gg \phi_{22}$ and $a \sim 0$ give $D_{\rm T}^{xx}/D_{\rm T}^{yy} \sim \xi_\mu^{2/3} \ll 1$, independent of N. This is analogous to the result $D_{\rm T}^{xx}/D_{\rm T}^{yy} \sim \xi_\nu^{2/3} \ll 1$ obtained in the unstratified case (Kim 2005). In this case, the anisotropy in the transport is caused solely by shear stabilisation. For an isotropic forcing with $\phi_{11} \sim \phi_{22}$ and $a \sim 1$, $D_{\rm T}^{xx}/D_{\rm T}^{yy} \sim (\mathcal{A}/N)^2(\nu/\mu)^{2/3}\xi_\nu \ll 1$. In other words, the anisotropy in turbulent transport depends on stratification, shear, and ν/μ, as clearly shown in Table 1. Since $(\mathcal{A}/N)^2 \ll 1$ and $\nu/\mu \ll 1$ in the tachocline, $D_{\rm T}^{xx}/D_{\rm T}^{yy}$ is much smaller than $\xi_\nu^{2/3}$ obtained in the unstratified case (Kim 2005). That is, the anisotropy in transport is further enhanced due to stratification. We emphasise that the anisotropy in turbulent transport is much stronger than that in turbulence amplitude, as discussed previously (see also Table 1). This result also shows the reduction in $D_{\rm T}^{xx}$ for large μ and again highlights the importance of the radiative damping in reducing the vertical transport, thereby increasing the anisotropy in the transport.

Finally, Eq. (31) demonstrates one of the most important effects of a stable stratification, which is to drive a system away from a uniform rotation with a negative eddy viscosity. Recall that, in the absence of stratification, the eddy viscosity is positive in 3D while negative in the 2D limit (e.g. see Kim 2005). In contrast, the eddy viscosity in Eq. (31) is negative in both the 2D ($\beta = 0$ and $\gamma = 1$) and 3D cases. This behaviour was also found in recent numerical simulations by Miesch (2003) of a stably stratified turbulence with an imposed shear driven by penetrative convection, who found anti-diffusive radial and diffusive latitudinal momentum transport. Anti-diffusive momentum transport is a generic feature of a strongly stratified medium (i.e. a geophysical system). It is interesting to note that a negative viscosity was also found in the previous work on momentum transport due to radiatively damped gravity waves (e.g. Kim & MacGregor 2001, 2003). In addition, the result (31) shows that the (anti-diffusive) momentum transport becomes less efficient for strong stratification (large N), in agreement with Miesch (2003).

To summarise, our results show that the shearing effect by radial differential rotation, together with gravity waves, is an important mechanism for turbulence regulation, leading to a weak turbulent transport and anisotropic turbulence and transport in the tachocline. Furthermore, we have consistently derived the values of turbulence level, particle mixing, and momentum transport starting from the first principle, clearly identifying the different roles of gravity waves and shearing in transport. For instance, in comparison with Chaboyer & Zahn (1992) or Spiegel & Zahn (1992), which start with the assumption of a strong horizontal mixing, we identified the source of this anisotropic turbulence. In particular, we made a clear distinction between the anisotropy in the turbulence level and turbulent transport.

4. Discussion and conclusions

We have studied turbulent transport in the stably stratified tachocline with a strong radial differential rotation, when turbulence is driven and maintained by a forcing (e.g. due to plumes penetrating from the convection zone or due to instability). We assumed that both turbulence and gravity waves are on small scales (with no clear scale separation between the two) and treated the interaction among gravity waves, turbulence, and shear flow consistently. Unlike a shear flow, which quenches both turbulence level and transport, a stable stratification is shown to mainly inhibit turbulent transport, leading to a further reduction in transport compared to the unstratified case (Kim 2005). Specifically, for parameter values typical of the tachocline ($N/\mathcal{A} \gg 1$), particle transport due to a strong radial forcing ϕ_{11} (with $\phi_{22} = 0$) is reduced as $\xi_D\xi_\mu^{-2/3}N^{-2}$, becoming much smaller than horizontal transport ($\propto\xi_D\xi_\mu^{-4/3}N^{-2}$) by a factor of $\xi_\mu^{2/3} \ll 1$. Here, $\xi_\nu = \nu k_y^2/\mathcal{A} \ll 1$, $\xi_D = Dk_y^2/\mathcal{A} \ll 1$, and $\xi_\mu = \mu k_y^2/\mathcal{A} \ll \xi_\nu$ are the small parameters characterising a strong shear limit (see the main text for more details). Note that in this case $D_{\rm T}^{xx}/D_{\rm T}^{yy} \propto \xi_\mu^{2/3} \ll 1$ depends only on shearing but not on stratification, indicating that the anisotropy in particle transport is mainly governed by radial differential rotation. A similar scaling ($\propto\xi_\nu^{2/3} \ll 1$) was also found in the unstratified case (Kim 2005). However, in the case of an isotropic forcing with $\phi_{11} \sim \phi_{22}$ and $k_x/k_y \sim 1$, the horizontal mixing is much less reduced with $D_{\rm T}^{yy} \sim \mathcal{A}^{-2}\xi_\nu^{-2/3}$ (with no effect of stratification), leading to a stronger anisotropy in transport with $D_{\rm T}^{xx}/D_{\rm T}^{yy} \sim (\mathcal{A}/N)^2(\nu/\mu)^{2/3}\xi_\nu \ll \xi_\nu^{2/3} \ll 1$. Note that the anisotropy becomes stronger for larger μ.

Furthermore, the vertical momentum transport was shown to be anti-diffusive with a negative eddy viscosity. That is, small-scale turbulence influenced by gravity waves accentuates the gradient in a radial differential rotation rather than making it uniform. This is similar to the tendency obtained in the case of momentum deposition by gravity waves due to radiative damping (Kim & MacGregor 2001, 2003). The sharpening of the gradient of the radial shear due to the negative viscosity could eventually lead to time variation in the tachocline (similar to Kim & MacGregor 2001) or instability (e.g., see Petrovay 2003), causing a rapid radial mixing and thus reducing the anisotropy.

Even in the stably stratified radiative interiors of stars, as well as in the tachocline, background turbulence has often been assumed to be present to enhance the value of effective viscosity. While the clarification of the source of turbulence responsible for such an enhanced eddy viscosity is an interesting problem, our results demonstrate how this residual turbulence interacts with gravity waves and shear flow, providing the prediction for the values of eddy viscosity, as well as of the particle diffusivity, that depend on physical quantities like $\mathcal{A}$ and N. In particular, the radial particle transport $D_{\rm T}^{xx} \sim \xi_D \xi_\mu^{-2/3} N^{-2}$ indicates that turbulent transport of particles can be inhibited due to stable stratification, shear flow, and large radiative damping. This finding can have interesting implications for the surface depletion of lithium in the Sun and other stars (i.e., Pinsonneault 1997), which will be studied in a future publication. Furthermore, if a similar physical process operates in the bulk of the radiative interior of the sun, a negative viscosity that we obtain implies that a radial differential rotation created during its spin-down would not be eliminated.

The tachocline is believed to possess strong toroidal magnetic fields of strength $10^4 \sim 10^5$ G, which could influence strongly turbulent transport in that region. This is an important problem since the presence of a weak poloidal magnetic field in the radiative interior, together with a strong toroidal magnetic field in the tachocline (acting as a boundary layer between the radiative interior and convection zone), could offer a mechanism for a uniform rotation in the interior, as well as for the tachocline confinement (e.g. Rüdiger & Kichatinov 1996; MacGregor & Charbonneau 1997; Gough & McIntyre 1998); see, however, Brun & Zahn (2006) for a negative result on this scenario. In this case, the values for the effective diffusivity of magnetic fields and eddy viscosity play a crucial role in determining the thickness of the tachocline. Therefore, a consistent computation of magnetic diffusivity and eddy viscosity with their dependences on physical quantities, such as the strength of magnetic fields, the Brunt-Väisälä frequency, and shearing rate, would be of primary interest (Kim & Leprovost 2007). It is an interesting question, in general, whether a negative eddy viscosity, favoured in a stably stratified medium, remains a robust feature in the presence of magnetic field in view of the forward energy cascade (i.e. positive eddy viscosity) in MHD turbulence. Furthermore, composition gradients (discussed in Sect. 3) and meridional flows would contribute to the transport in the tachocline. In particular, meridional flows are expected to enhance the radial transport of chemical species by advection, as discussed in Kim (2005), although this enhancement would be reduced for stronger horizontal turbulent; e.g., see Kim (2005) and Chaboyer & Zahn (1992). These issues are, however, outside the scope of this paper and will be addressed in a future publication.

Acknowledgements. This work was supported by the UK PPARC grant PP/B501512/1.

References

Brummell, N. H., Clune, T. L., & Toomre, J. 2002, ApJ, 570, 825
Brun, A. S., & Zahn, J.-P. 2006, A&A, 457, 665
Brun, A. S., Turck-Chiéze, S., & Zahn, J.-P. 1999, ApJ, 25, 1032
Burrell, K. H. 1997, Phys. Plasmas, 4, 1499
Chaboyer, B., & Zahn, J.-P. 1992, A&A, 253, 173
Charbonneau, P., Tomczyk, S., Schou, J., & Thompson, M. J. 1998, ApJ, 527, 445
Charbonneau, P., Dikpati, M., & Gilman, P. A. 1999, ApJ, 526, 523
Charbonnel, C., & Talon, S. 2005, Science, 309, 2189
Corbard, T., Blanc-Féraud, L., Berthomieu, G., & Provost, J. 1999, A&A, 344, 696
García López, R. J., & Spruit, H. C. 1991, A&A, 377, 268
Gilman, P. A. 2000, Sol. Phys., 192, 27
Gough, D. O., & McIntyre, M. E. 1998, Nature, 394, 755
Jacobitz, F. G., Sarkar, S., & Van Atta, C. W. 1997, J. Fluid Mech., 342, 231
Kim, E. 2004, Mod. Phys. Lett. B, 18, 1
Kim, E. 2005, A&A, 441, 763
Kim, E. 2006, Phys. Rev. Lett., 96, 084504
Kim, E., & Leprovost, N. 2007, A&A, 465, 633
Kim, E., & MacGregor, K. B. 2001, ApJ, 556, L117
Kim, E., & MacGregor, K. B. 2003, ApJ, 588, 645
Kosovichev, A. G. 1996, ApJ, 469, L61
Leprovost, N., & Kim, E. 2006, A&A, 456, 617
Lighthill, M. J. 1978, Waves in Fluids (Cambridge: Cambridge Univ. Press)
MacGregor, K. B., & Charbonneau, P. 1999, ApJ, 519, 911
Michaud, G., & Zahn, J.-P. 1998, Theoret. Comput, Fluid Dynamics, 11, 183
Miesch, M. S. 2003, ApJ, 586, 663
Miesch, M. S., Brun, A. S., & Toomre, J. 2006, ApJ, 641, 618
Petrovay, K. 2003, Sol. Phys., 215, 17
Pinsonneault, M. 1997, ARA&A, 35, 357
Plumb, R. A. 1977, J. Atmos. Sci., 34, 1847
Press, W. H. 1981, ApJ, 245, 286
Press, W. H., & Rybicki, G. B. 1981, ApJ, 248, 751
Rogers, T. M., & Glatzmaier, G. A. 2005, ApJ, 620, 432
Rüdiger, G., & Kitchatinov, L. L. 1996, ApJ, 466, 1078
Schatzman, F. D. 1993, The stars (Berlin, London: Springer-Verlag)
Schatzman, F. D., Zahn, J.-P., & Morel, P. 2000, A&A, 364, 876
Spiegel, E. A., & Zahn, J.-P. 1992, A&A, 265, 106
Stacey, M. T., Monismith, S. G., & Burau, J. R. 1999, J. Phys. Oceanography, 29, 1950
Stix, M. 1989, The sun: an introduction (Berlin, London: Springer-Verlag)
Talon, S., Kumar, P., & Zahn, J.-P. 2002, ApJ, 574, L175
Watson, M. 1981, Geophys. Astrophys. Fluid Dynamics, 16, 285

Online Material

Appendix A:

In this Appendix, we show how to derive Eqs. (26)–(31). To this end, we use $U_0(x)\hat{y} = -x\mathcal{A}\hat{y}$ in Eqs. (1)–(4), and introduce the transforms $\hat{w}$ and $\hat{\tilde{w}}$ for $w = v_i, n, p, h_i$, and f as follows:

$$\begin{aligned}\hat{w} &\equiv \tilde{w}\exp\left[\nu(k_x^3/3k_y\mathcal{A} + k_{\rm H}^2 t)\right],\\ \hat{\tilde{w}} &\equiv \tilde{w}\exp\left[\mu(k_x^3/3k_y\mathcal{A} + k_{\rm H}^2 t)/2\right],\end{aligned} \tag{A.1}$$

where $k_{\rm H}^2 = k_y^2 + k_z^2$. We then use a new time variable $\tau = k_x/k_y + \mathcal{A}t$ to rewrite Eqs. (1)–(4) as:

$$\mathcal{A}\partial_\tau\hat{v}_x = -{\rm i}\tau k_y\hat{p} - g\hat{\rho} + \hat{f}_x, \tag{A.2}$$

$$\mathcal{A}\partial_\tau\hat{v}_y - \mathcal{A}\hat{v}_x = -{\rm i}k_y\hat{p} + \hat{f}_y, \tag{A.3}$$

$$\mathcal{A}\partial_\tau\hat{v}_z = -{\rm i}k_z\hat{p} + \hat{f}_z, \tag{A.4}$$

$$0 = \tau\hat{v}_x + \hat{v}_y + \frac{k_z}{k_y}\hat{v}_z, \tag{A.5}$$

$$\mathcal{A}[\partial_\tau + \xi_\mu(\gamma+\tau^2)]\tilde{\rho} = \frac{N^2}{g}\tilde{v}_x, \tag{A.6}$$

$$\mathcal{A}[\partial_\tau + \xi_D(\gamma+\tau^2)]\tilde{n} = -(\partial_x n_0)\tilde{v}_x. \tag{A.7}$$

For a strong shear limit where $\mu = \mu k_y^2/\mathcal{A} \ll 1$, Eqs. (A.2)–(A.6) can be combined to yield the equation for $\hat{\tilde{\rho}}$ as

$$\partial_\tau[(\gamma+\tau^2)\partial_\tau\hat{\tilde{\rho}}] + \frac{\gamma N^2}{\mathcal{A}^2}\hat{\tilde{\rho}} \simeq \frac{N^2}{g\mathcal{A}^2}\hat{\tilde{h}}_1(\tau), \tag{A.8}$$

to leading order in $\xi_\mu = \mu k_y^2/\mathcal{A} \ll 1$. Here, $\hat{\tilde{h}}_1(\tau) = \gamma\hat{\tilde{h}}_x - \tau\hat{\tilde{h}}_y - \tau\beta\hat{\tilde{h}}_z$; $\gamma = 1+\beta^2$ and $\beta = k_z/k_y$. In the limit of $N^2/\mathcal{A}^2 \gg 1$, Eq. (A.8) can be solved with the following solutions valid up to $\mathrm{O}(\overline{N}^{-2})$:

$$\begin{aligned}\hat{\tilde{\rho}}(\tau) &= \frac{N_*^2}{\overline{N}\mathcal{A}}\frac{1}{(\gamma+\tau^2)^{1/4}}\int^\tau\frac{{\rm d}\tau_1}{(\gamma+\tau_1^2)^{1/4}}\sin\left[\varphi(\tau)-\varphi(\tau_1)\right]\hat{\tilde{h}}_1(\tau_1),\\ \hat{\tilde{v}}_x(\tau) &= \frac{1}{\overline{N}\mathcal{A}}\frac{1}{(\gamma+\tau^2)^{5/4}}\int^\tau\frac{{\rm d}\tau_1}{\varpi(\tau_1)(\gamma+\tau_1^2)^{1/4}}\Big[-\frac{\tau}{2}\sin\left[\varphi(\tau)\right.\\ &\quad\left.-\varphi(\tau_1)\right] + \overline{N}\sqrt{\gamma+\tau^2}\varpi(\tau)\cos\left[\varphi(\tau)-\varphi(\tau_1)\right]\Big]\hat{\tilde{h}}_1(\tau_1),\\ \hat{\tilde{v}}_y(\tau) &= -\frac{\tau}{\gamma}\hat{\tilde{v}}_x(\tau) + \frac{\beta^2}{\mathcal{A}\gamma}\hat{\tilde{\rho}}(\tau) - \frac{\beta}{\gamma\mathcal{A}}\int^\tau{\rm d}\tau_1\overline{G}(\tau,\tau_1)\hat{\tilde{h}}_2(\tau_1),\\ \hat{\tilde{v}}_z(\tau) &= -\frac{\tau\beta}{\gamma}\hat{\tilde{v}}_x(\tau) - \frac{\beta}{\mathcal{A}\gamma}\hat{\tilde{\rho}}(\tau) + \frac{1}{\gamma\mathcal{A}}\int^\tau{\rm d}\tau_1\overline{G}(\tau,\tau_1)\hat{\tilde{h}}_2(\tau_1).\end{aligned} \tag{A.9}$$

Here, again $\beta = k_z/k_y$, $\gamma = 1+\beta^2$; $N_*^2 = N^2/g\mathcal{A}$, $\overline{N}^2 = N^2\gamma/\mathcal{A}^2$; $\overline{G}(\tau,\tau_1) = \exp\left\{(\xi_\mu/2 - \xi_\nu)[(\gamma\tau+\tau^3/3) - (\gamma\tau_1+\tau_1^3/3)]\right\}$; $\xi_\nu = \nu k_y^2/\mathcal{A}$;

$$\begin{aligned}\hat{\tilde{h}}_1 &= (1+\beta^2)\hat{\tilde{h}}_x - \tau_1\hat{\tilde{h}}_y - \tau_1\beta\hat{\tilde{h}}_z,\\ \hat{\tilde{h}}_2 &= -\beta\hat{\tilde{h}}_y + \hat{\tilde{h}}_z,\\ \varphi(\tau) &= \frac{\overline{N}\alpha}{2}\ln\frac{\sqrt{\gamma+\tau^2}+\tau}{\sqrt{\gamma+\tau^2}-\tau} - \frac{1}{8\overline{N}}\frac{\tau}{\sqrt{\gamma+\tau^2}},\\ \varpi(\tau) &= \alpha - \frac{1}{8\overline{N}^2}\frac{\gamma}{\gamma+\tau^2},\\ \alpha &= 1 - \frac{1}{8\overline{N}^2}.\end{aligned} \tag{A.10}$$

By following an algebra similar to the one used in Kim (2005) and by using the correlation function of the forcing given in Eq. (20), we can obtain the following correlation fictions $\langle v_i v_j\rangle$ to leading orders in $1/\overline{N}^2 \ll 1$ and $\xi_\mu = \mu k_y^2/\mathcal{A} \ll 1$:

$$\begin{aligned}\langle v_x^2\rangle &\sim \frac{\tau_f}{2\mathcal{A}}\int\frac{{\rm d}^3k{\rm d}\tau}{(2\pi)^3}\frac{\phi_{11}(\boldsymbol{k})}{\sqrt{\gamma+a^2}}\frac{{\rm e}^{-\xi_\mu Q(\tau,a)}}{(\gamma+\tau^2)^{3/2}}\\ &\quad\times\left[1+\cos\left[2(\varphi(\tau)-\varphi(a))\right]\right],\end{aligned} \tag{A.11}$$

$$\begin{aligned}\langle v_y^2\rangle &\sim \frac{\tau_f}{\mathcal{A}}\int\frac{{\rm d}^3k{\rm d}\tau}{(2\pi)^3}\Big[{\rm e}^{-\xi_\mu Q(\tau,a)}\frac{\phi_{11}(\boldsymbol{k})}{2\sqrt{\gamma+a^2}}\frac{\tau^2}{\gamma^2(\gamma+\tau^2)^{3/2}}\\ &\quad+{\rm e}^{-2\xi_\nu Q(\tau,a)}\frac{\beta^2\phi_{22}(\boldsymbol{k})}{\gamma^2}\Big],\end{aligned} \tag{A.12}$$

$$\begin{aligned}\langle v_z^2\rangle &\sim \frac{\tau_f}{\mathcal{A}}\int\frac{{\rm d}^3k{\rm d}\tau}{(2\pi)^3}\Big[{\rm e}^{-\xi_\mu Q(\tau,a)}\frac{\phi_{11}(\boldsymbol{k})}{2\sqrt{\gamma+a^2}}\frac{\tau^2\beta^2}{\gamma^2(\gamma+\tau^2)^{3/2}}\\ &\quad+{\rm e}^{-2\xi_\nu Q(\tau,a)}\frac{\phi_{22}(\boldsymbol{k})}{\gamma^2}\Big],\end{aligned} \tag{A.13}$$

$$\begin{aligned}\langle v_x v_y\rangle &\sim -\frac{\tau_f}{\mathcal{A}\gamma\overline{N}^2}\int\frac{{\rm d}^3k{\rm d}\tau}{(2\pi)^3}\frac{\phi_{11}(\boldsymbol{k})}{\sqrt{\gamma+a^2}\varpi(a)^2}\frac{{\rm e}^{-\xi_\mu Q(\tau,a)}\tau}{(\gamma+\tau^2)^{5/2}}\\ &\quad\times\Big[-\frac{\tau}{2}\sin\left[\varphi(\tau)-\varphi(a)\right] + \overline{N}\sqrt{\gamma+\tau^2}\varpi(\tau)\\ &\quad\times\cos\left[\varphi(\tau)-\varphi(a)\right]\Big]^2.\end{aligned} \tag{A.14}$$

Here, $a = k_x/k_y$, $Q(\tau,a) = (\gamma\tau+\tau^3/3) - (\gamma a + a^3/3)$; spatial symmetries $\psi_{ij}(k_y) = \psi_{ij}(-k_y)$ and $\psi_{ij}(k_z) = \psi_{ij}(-k_z)$ are used. We then compute τ integrals in Eq. (A.14) in the strong shear limit $\xi_\nu \ll \xi_\mu \ll 1$ and use $\langle v_x v_y\rangle = -\nu_{\rm T}^{xx}\partial_x U_0 = \nu_{\rm T}^{xx}\mathcal{A}$ to obtain Eqs. (26)–(28) and (31).

Next, to compute particle transport, we integrate Eq. (A.7) in time to obtain

$$\begin{aligned}\tilde{n}(\boldsymbol{k}(t),t) = -\partial_i n_0\int{\rm d}t_1{\rm d}^3k_1\hat{g}(\boldsymbol{k},t;\boldsymbol{k}_1,t_1)\\ \times{\rm e}^{-DQ(t,t_1)}\tilde{v}_i(\boldsymbol{k}_1,x,t_1).\end{aligned} \tag{A.15}$$

Here, $Q(t,t_1) = \int_{t_1}^t{\rm d}t'[k_x^2(t') + k_{\rm H}^2] = [k_x^3 - k_{1x}^3]/3k_y\mathcal{A} + k_{\rm H}^2(t-t_1)$; $k_{\rm H}^2 = k_y^2 + k_z^2$ is the amplitude of wave number in the horizontal plane; $k^2 = k_{\rm H}^2 + k_x^2$; $\hat{g}$ is the Green's function given by

$$\begin{aligned}\hat{g}(\boldsymbol{k},t;\boldsymbol{k}_1,t_1) &= \delta(k_y - k_{1y})\delta(k_z - k_{1z})\\ &\quad\times\delta\left[k_x - k_{1x} - k_{1y}(t-t_1)\mathcal{A}\right].\end{aligned}$$

A similar analysis using Eqs. (A.9), (A.16), (11)–(13), and (20) and $\langle n v_i\rangle = -D_{ij}\partial_j n_0$ gives

$$\begin{aligned}D_{\rm T}^{xx} &= \frac{\tau_f}{2(2\pi)^3\mathcal{A}^2\overline{N}^2}\int{\rm d}^3k{\rm d}\tau\frac{\xi_D\phi_{11}(\boldsymbol{k}){\rm e}^{-\xi_\mu Q(\tau,a)}}{\sqrt{\gamma+a^2}}(\gamma+\tau^2)^{1/2},\\ D_{\rm T}^{yy} &= \frac{\tau_f}{(2\pi)^3\mathcal{A}^2}\int{\rm d}^3k{\rm d}\tau\frac{\xi_D}{\gamma^2}\Big[{\rm e}^{-\xi_\mu Q(\tau,a)}\frac{\phi_{11}(\boldsymbol{k})\tau^2\sqrt{\gamma+\tau^2}}{2\overline{N}^2\sqrt{\gamma+a^2}}\\ &\quad+{\rm e}^{-2\xi_\nu Q(\tau,a)}\beta^2\phi_{22}(\boldsymbol{k})(\tau-a)^2\left(\gamma+\tau^2\right)\Big].\end{aligned} \tag{A.16}$$

Here, $\xi_D = Dk_y^2/\mathcal{A} \sim \xi_\nu \ll 1$. Finally, the evaluation of τ integrals in Eq. (A.16) gives us Eqs. (29)–(31) in the main text.